Electronic Supplementary Material (ESI) for Journal of Materials Chemistry C.

Supporting Information

Gd-Er interaction promotes $NaGdF_4$: Yb, Er as a new candidate for high-power density applications

Daniel Avram[*,a], *Andrei A. Patrascu*[a, b], *Marian Cosmin Istrate*[c, d], *and Carmen Tiseanu*[*, a]

[a]*National Institute for Laser, Plasma and Radiation Physics, 409 Atomistilor Street, 077125 Magurele-Ilfov, Romania*
[b]*"C. D. Nenitzescu" Institute of Organic and Supramolecular Chemistry of the Romanian Academy, Splaiul Independentei 202B, Bucharest 020464, Romania*
[c]*National Institute of Materials Physics, 405A Atomistilor Street, 077125 Magurele-Ilfov, Romania*
[d]*University of Bucharest, Faculty of Physics, 077125 Magurele, Romania*
[*] *E-mail: radu.avram@inflpr.ro; carmen.tiseanu@inflpr.ro*

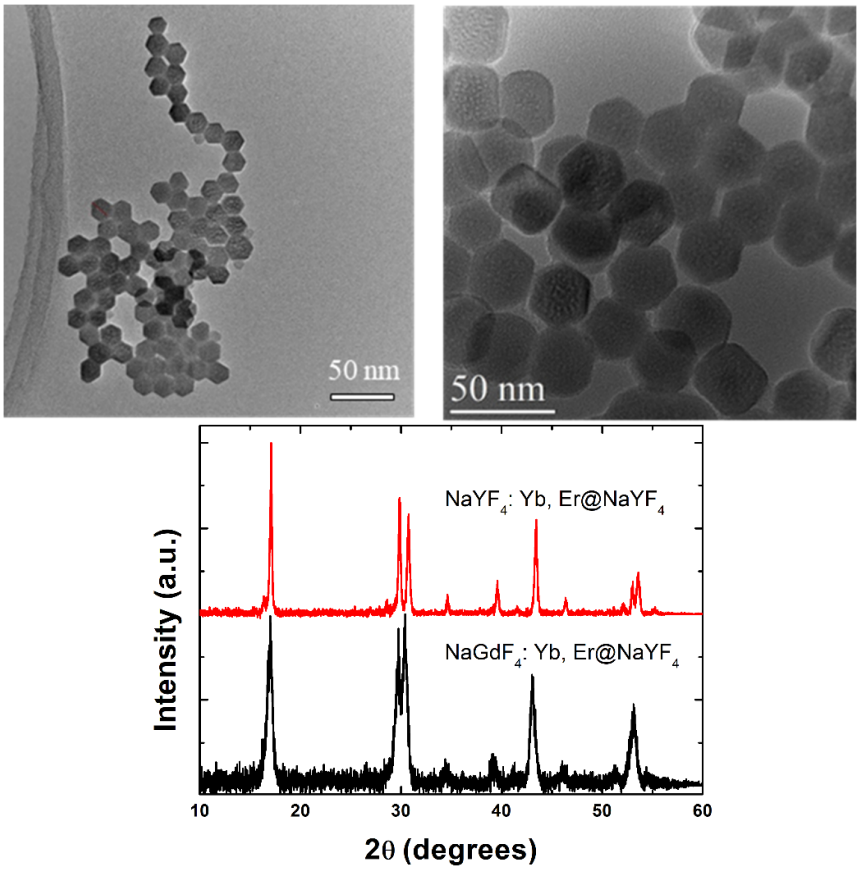

Figure S1. TEM images of $NaGdF_4$:Yb, Er@$NaYF_4$ (left) and $NaYF_4$:Yb, Er@$NaYF_4$ (right) nanoparticles after decapping and redispersing them in water. XRD of $NaYF_4$:Yb, Er@$NaYF_4$ and $NaGdF_4$:Yb, Er@$NaYF_4$ (bottom).

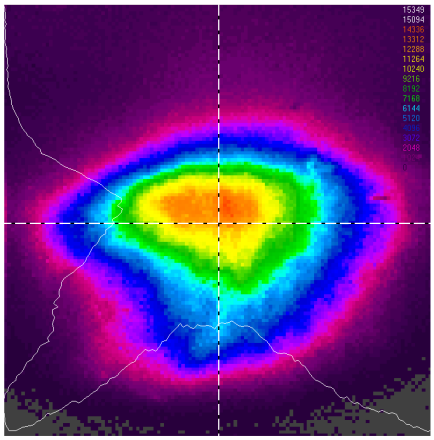

Figure S2. The beam profile of the pulsed laser excitation spot measured with a Pyrocam III (Ophir Spiricon).

The shape of the laser beam profile is Gaussian, with a width of 10 mm on X scale and 8 mm on Y scale, as expected of an OPO (Optical Parametric Oscillator) laser system. A Gaussian profile of the energy distribution leads to the fact that particles at different positions within the laser beam experience different excitation power densities and consequently yield different emission intensity[1]. As the beam profile is rather different from a perfect Gaussian profile, all the emission intensity measurements are not compensated for the shape of the beam profile. All energy dependence measurements were performed under identical experimental conditions to have meaningful relative values for comparison purposes.

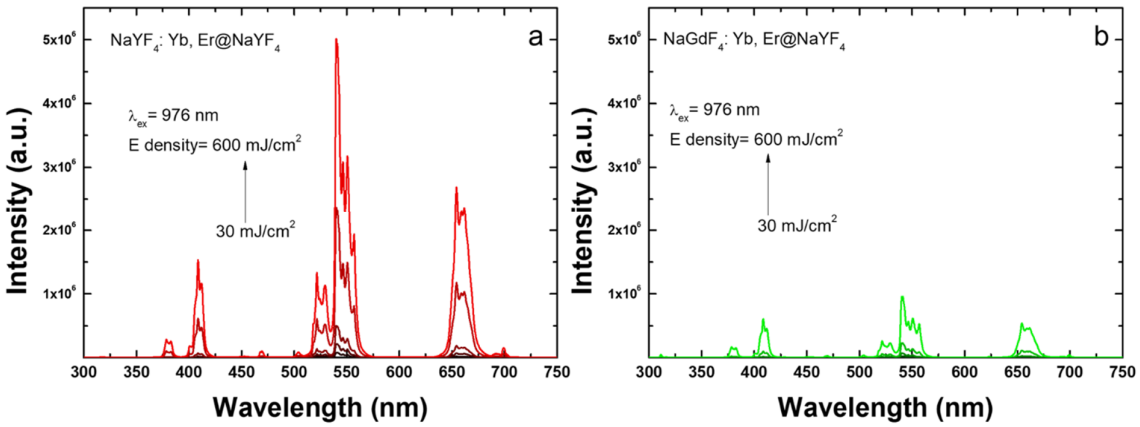

Figure S3. Energy density dependencies of Er UC emission spectra of $NaYF_4$:Yb, Er@$NaYF_4$ (a) and $NaGdF_4$:Yb, Er@$NaYF_4$ (b). The emission spectra are not normalized for comparison purposes.

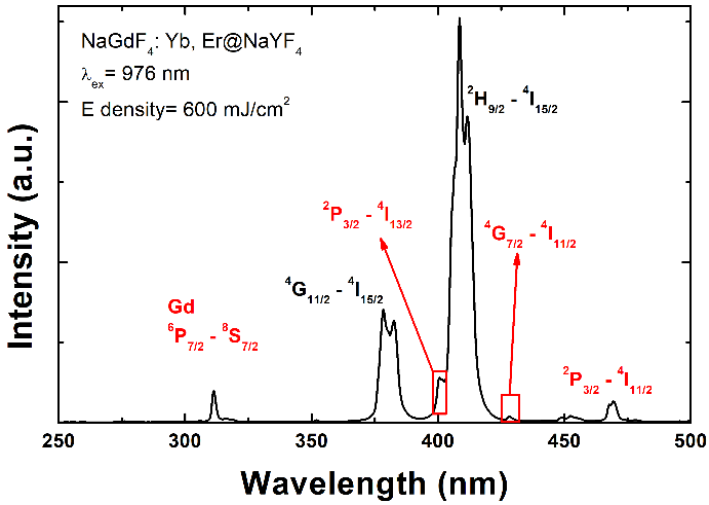

Figure S4. The upconversion emission spectrum of for $NaGdF_4$:Yb, Er@$NaYF_4$ in the 250 – 500 nm spectral range upon pulsed excitation at 976 nm with 600 mJ/cm^2 energy density. The emission spectrum was measured at 0.1 µs delay after the laser pulse and 1 ms gate width. The fourth-order UC emission of Er at 400 nm ($^2P_{3/2} \rightarrow {}^4I_{13/2}$), 427 nm ($^4G_{7/2} \rightarrow {}^4I_{11/2}$) and 468 nm ($^2G_{7/2} \rightarrow {}^4I_{13/2}$; $^2P_{3/2} \rightarrow {}^4I_{11/2}$) and Gd ($^6P_{7/2}$-$^8S_{7/2}$) emissions denoted with red font in the Figure.

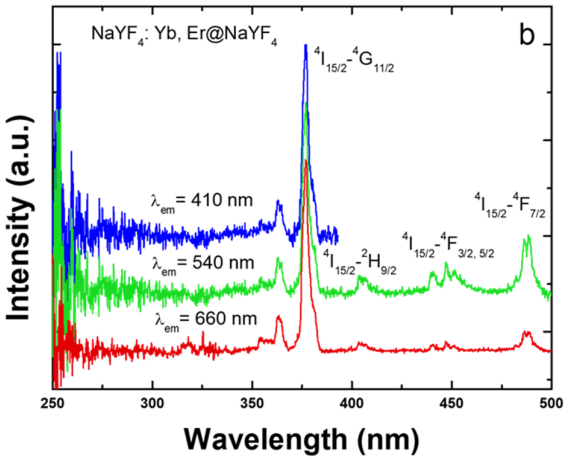

Figure S5. Excitation spectra of Er and Gd emissions in $NaYF_4$:Yb, Er@$NaYF_4$ (b) . The monitored emissions are denoted in the Figure.

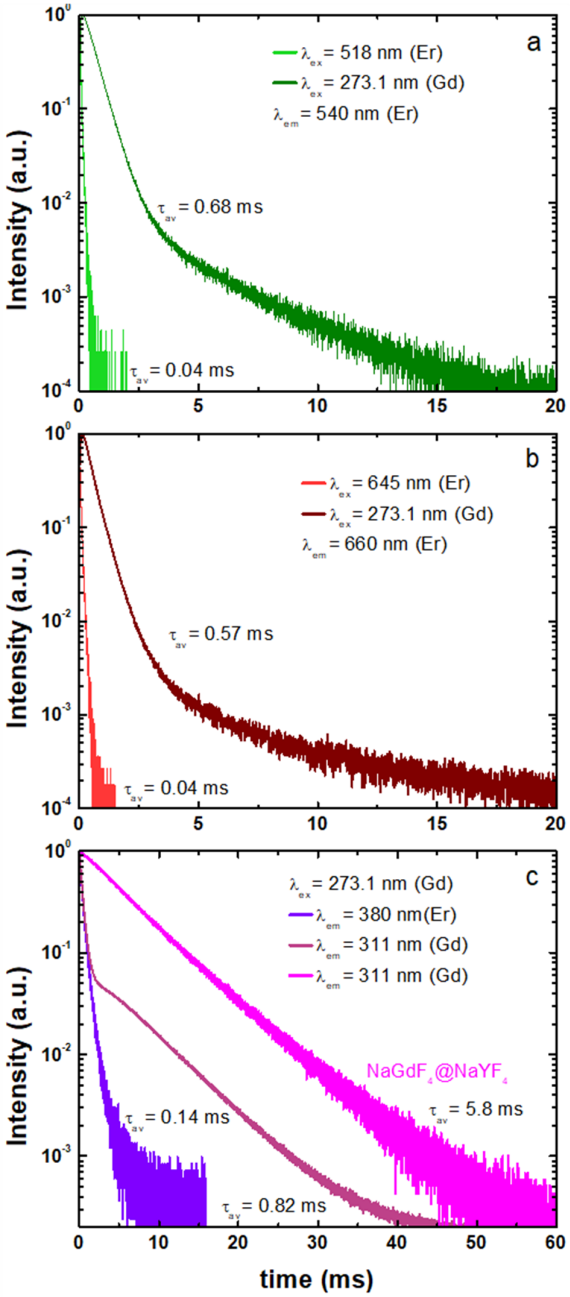

Figure S6. Comparison between Er emission decays at 540 ($^2S_{3/2}$-$^4I_{15/2}$) and 660 nm ($^4F_{9/2}$-$^4I_{15/2}$) measured under Gd (273.1 nm, $^8S_{7/2}$-$^6I_{7/2}$) and direct Er absorption at 518 and 645 nm (corresponding to $^4I_{15/2}$-$^2H_{11/2}$ and $^4I_{15/2}$-$^4F_{9/2}$ absorption transitions). The Gd emission decay is also included (excitation at 273.1 nm, emission at 311 nm) from $NaGdF_4$: Yb, Er@$NaYF_4$ and $NaGdF_4$@$NaYF_4$ for comparison with the Er emission at 380 nm ($^4G_{11/2}$-$^4I_{15/2}$). The average decay times, τ_{av}, with an error of ±0.005 ms) are included on the Figure.

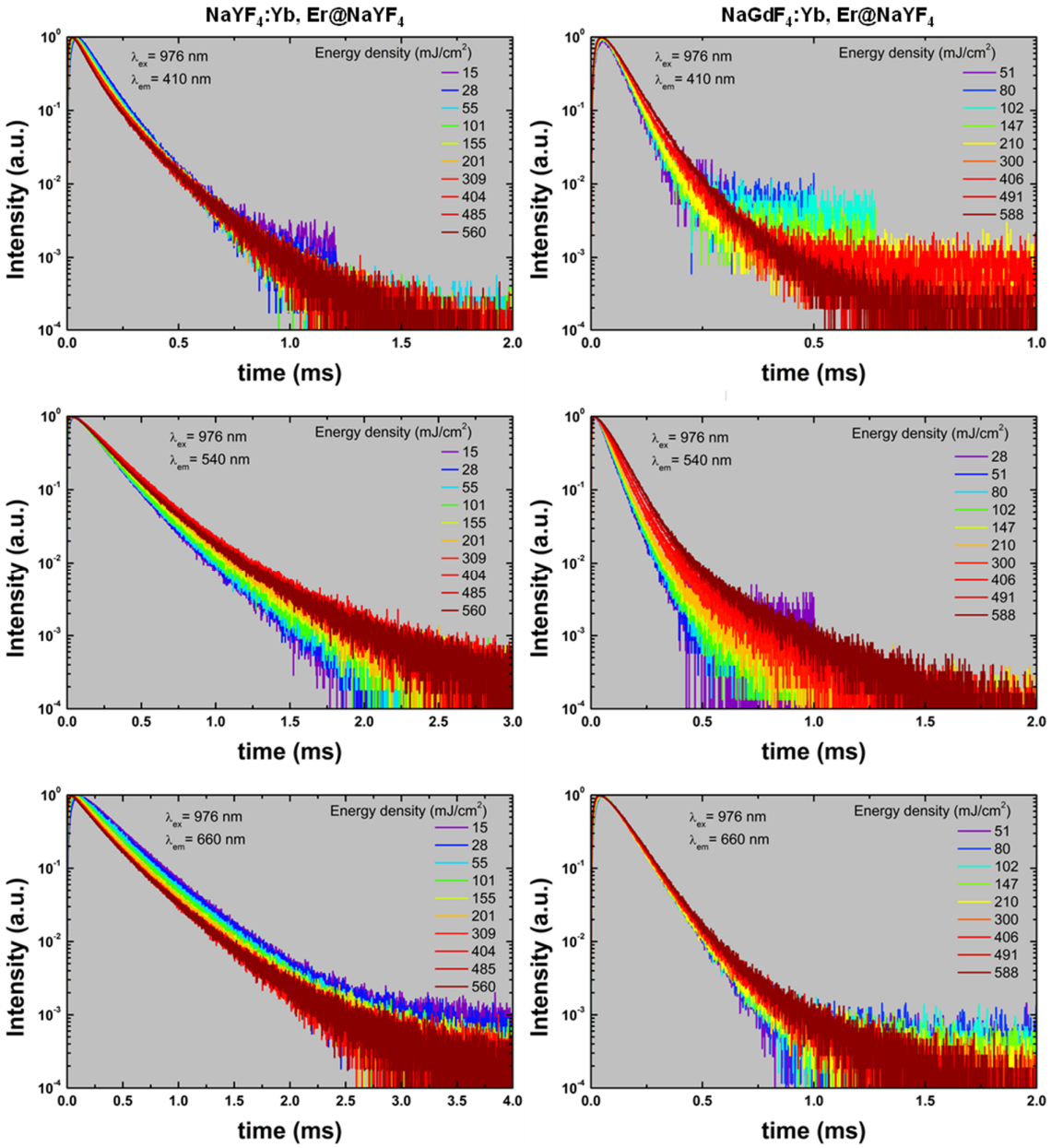

Figure S7. Evolution of Er UC emission decays of $NaYF_4$:Yb, Er@$NaYF_4$ and $NaGdF_4$:Yb, Er@$NaYF_4$ monitored at 410 ($^2H_{9/2}$-$^4I_{15/2}$), 540 ($^2H_{11/2}$, $^4S_{3/2}$ – $^4I_{15/2}$) and 660 nm ($^4F_{9/2}$-$^4I_{15/2}$) with energy density. Energy density varied from 15 to 600 mJ/cm^2, and excitation was performed at 976 nm. The emission decays are identical to those in Fig 6 but represented in a logarithmic Y scale.

Table S1. The rise and decay times of UC emission for $NaGdF_4$:Yb, Er@$NaYF_4$ (±0.003 ms) and $NaYF_4$:Yb, Er@$NaYF_4$ (±0.005 ms) are estimated as the single exponential fit from Figure 6. The fitting ranges were defined as follows: the rise time was fitted from the initial delay time to the delay of the maximum intensity, while the decay time was fitted from 95% of the maximum intensity until it dropped to the noise level defined.

$NaYF_4$:Yb, Er@$NaYF_4$

λ_{em}=	**410 nm**	**410 nm**	**540 nm**	**540 nm**	**650 nm**	**650 nm**
Energy density (mJ/cm^2)	**rise (10^{-3}ms)**	**decay (10^{-3}ms)**	**rise (10^{-3}ms)**	**decay (10^{-3}ms)**	**rise (10^{-3}ms)**	**decay (10^{-3}ms)**
15	19	99	11.9	184	42.4	324
28	18	98	10.4	187	33.2	310
55	15	97	85	188	26.9	300
101	12	96	6.5	196	18	288
155	9	97	4.9	207	14.1	273
201	8.8	95	4.1	218	12.4	271
309	7	94.8	3.2	226	94	259
404	6.6	88.6	2.4	235	77	254
485	6.1	88.4	2.35	225	67	256
560	5.5	88.3	2.3	214	56	257

$NaGdF_4$:Yb, Er@$NaYF_4$

λ_{em}=	**410 nm**	**410 nm**	**540 nm**	**540 nm**	**650 nm**	**650 nm**
Energy density (mJ/cm^2)	**rise (10^{-3}ms)**	**decay (10^{-3}ms)**	**rise (10^{-3}ms)**	**decay (10^{-3}ms)**	**rise (10^{-3}ms)**	**decay (10^{-3}ms)**
51	18	34	5.8	56	32.5	105.6
80	17	36	5.5	58	27.1	104.7
102	14.5	36.3	4.9	59.9	24.1	105.9
147	12.5	38.3	4.6	62.1	22.2	104
210	12.9	38.5	4.1	65.6	18.3	106
300	11	42	3.4	74.4	14.3	109
406	10	43.8	2.8	80.3	13.3	114
491	9.8	46.6	2.5	88.2	11.7	118.8
588	9.7	49.3	2.1	95.5	10	123.5

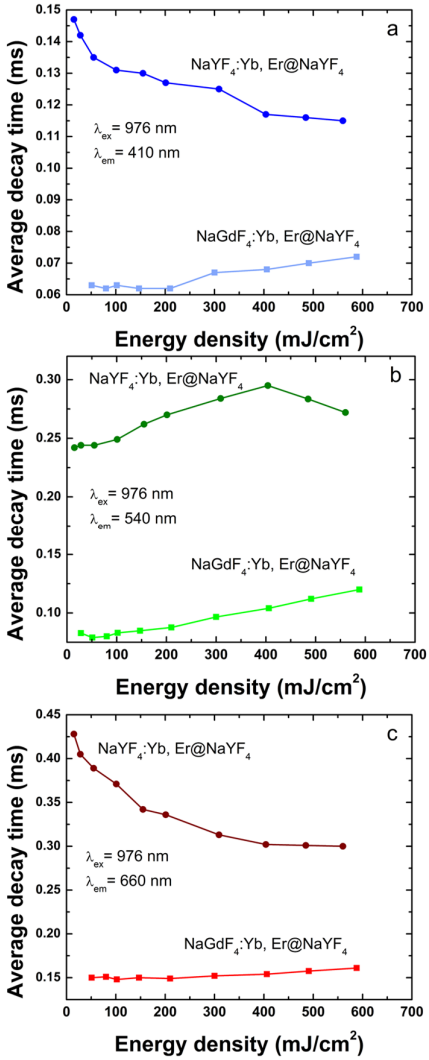

Figure S8. The average decay times of Er UC emission in $NaGdF_4$:Yb, Er@$NaYF_4$ (±0.003 ms) and $NaYF_4$:Yb, Er@$NaYF_4$ (±0.005 ms) calculated as the integrated area of the normalized emission decays.

Table S2. The average decay times of UC emission for $NaGdF_4$:Yb, Er@$NaYF_4$ (±0.003 ms) and $NaYF_4$:Yb, Er@$NaYF_4$ (±0.005 ms) were calculated as the integrated area of the normalised emission decays.

$NaYF_4$:Yb, Er@$NaYF_4$

Energy density (mJ/cm²)	λ_{em}=410 nm (10^{-3} ms)	λ_{em}=540 nm (10^{-3} ms)	λ_{em}=660 nm (10^{-3} ms)
15	147	242	428
28	142	244	405
55	135	244	389
101	131	249	371
155	130	262	342
201	127	270	336
309	125	284	313
404	117	295	302
560	115	272	300

$NaGdF_4$:Yb, Er@$NaYF_4$

Energy density (mJ/cm²)	λ_{em}=410 nm (10^{-3} ms)	λ_{em54}10 nm (10^{-3} ms)	λ_{em}=660 nm (10^{-3} ms)
28	--	82.8	--
51	63	79	150
80	62	80	151
102	63	83	148
147	62	84.8	150
210	62	87.6	149
300	67	96.6	152
406	68	104	154
588	72	120	161

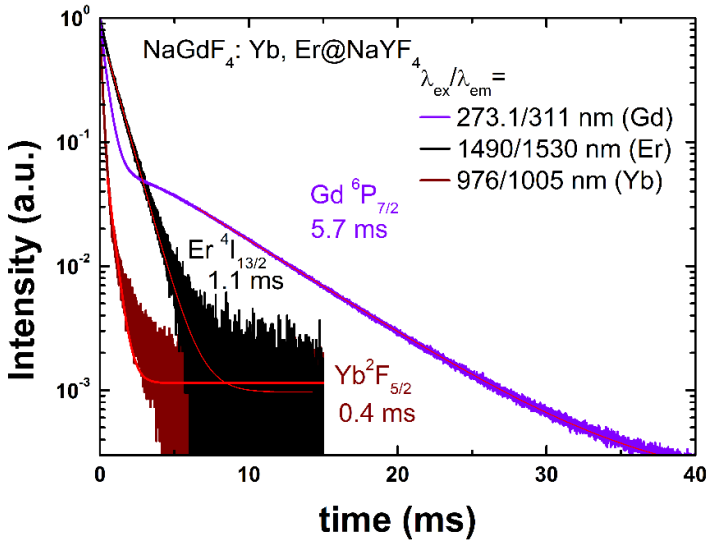

Figure S9. Comparison between Gd ($^6P_{7/2}$- $^8S_{7/2}$ at 311 nm), Yb ($^2F_{5/2}$ – $^2F_{7/2}$ at 1005 nm) and Er ($^4I_{13/2}$ – $^4I_{15/2}$ at 1530 nm) emission decays under direct excitation at 273.1, 976 and 1490 nm, respectively.

The emission decays were fitted using an exponential tail fit obtaining the decay times: 6.2 ms for Gd ($^6P_{7/2}$- $^8S_{7/2}$ at 311 nm), 0.17 ms for Yb ($^2F_{5/2}$ – $^2F_{7/2}$ at 1005 nm) and 1 ms for Er ($^4I_{13/2}$ – $^4I_{15/2}$ at 1530 nm). The Gd emission decay displays a fast and long component, with the fast component determined by the Gd-Er energy transfer [4-8].

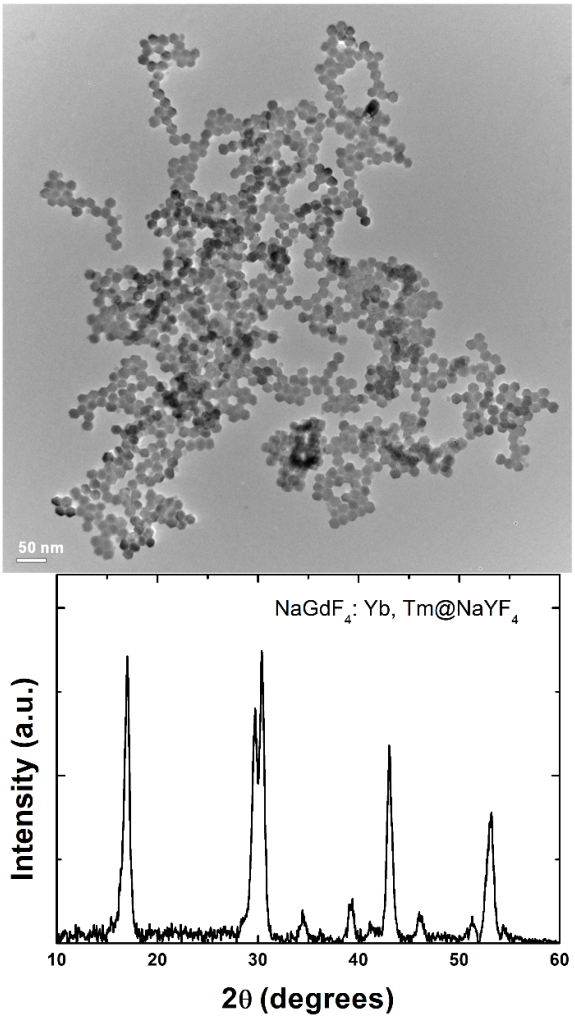

Figure S10. TEM image and XRD of $NaGdF_4$:Yb, Tm@$NaYF_4$ nanoparticles after decapping.

The water-dispersed $NaGdF_4$:Yb, Tm@$NaYF_4$ nanoparticles present a hexagonal phase and similar size of 18 nm to $NaGdF_4$:Yb, Er@$NaYF_4$.

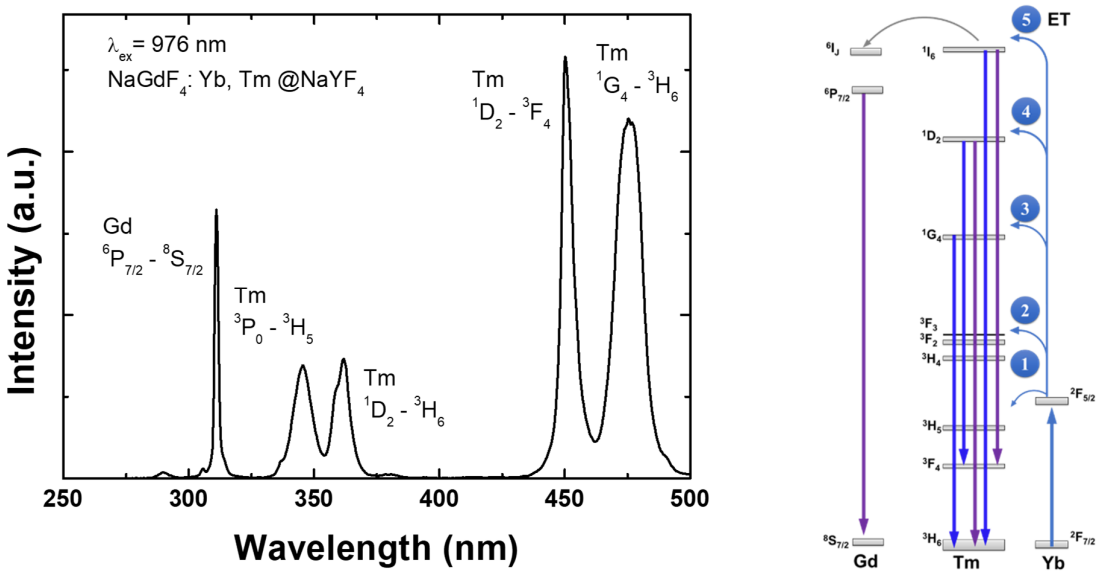

Figure S11 Upconversion emission spectrum of $NaGdF_4$:Yb, Tm@$NaYF_4$ upon 976 nm excitation at an energy density of 600 mJ/cm^2 (left panel). Schematic representation of the upconversion processes of $NaGdF_4$:Yb, Tm@$NaYF_4$ [9, 10]. The emission spectrum was measured at 0.1 µs delay after laser pulse and with 5 ms gate width.

Excitation into Yb absorption at 976 nm populates the $^2F_{5/2}$ level from $^2F_{7/2}$. Tm levels are populated following energy transfer from Yb up to 5 energy transfer upconversion (ETU) steps, Yb $^2F_{5/2}$ → Tm $^3H_5$, $^3F_2$, $^1G_4$, $^1D_2$ and $^1I_6$, respectively. Gd is then populated by energy transfer from Tm $^1I_6$ to Gd $^6P_{7/2}$ (**Figure S4**) [11]. The upconversion emission spectra of $NaGdF_4$:Yb, Tm@$NaYF_4$ present the characteristic Tm and Gd emission bands: $^1G_4$-$^3H_6$ at 475 nm, $^1D_2$-$^3F_4$ at 450 nm, $^1D_2$-$^3H_6$ at 365 nm, $^3P_0$-$^3H_5$ at 345 nm and $^6P_{7/2}$-$^8S_{7/2}$ (Gd) at 311 nm[11].

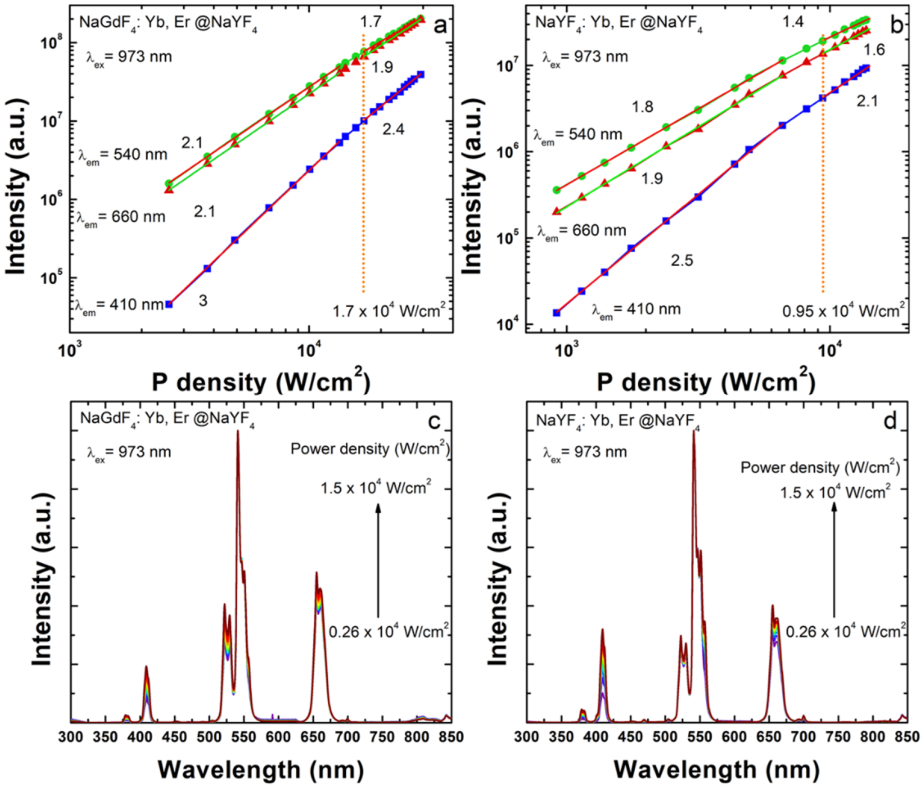

Figure S12. Power density dependencies of Er blue (410 nm), green (540 nm), and red (660 nm) UC emissions in $NaGdF_4$:Yb, Er@$NaYF_4$ and $NaYF_4$:Yb, Er@$NaYF_4$ upon laser diode excitation at 973 nm. Power density varied between ~ 0.26 and 1.5x10^4 W/cm^2. The laser diode is modulated with 1 ms pulse (square signal) at a 500 Hz frequency to diminish the laser heating effect [12]. The UC emission is monitored within the excitation pulse by use of 500 accumulations per emission spectrum.

The slopes of the power density agree with previous reports [13, 14]. The inflexion point, defined as the power density at which slopes diminish by ~20%, is greater, by a factor of 1.8, in $NaGdF_4$:Yb, Er@$NaYF_4$ compared to $NaYF_4$:Yb, Er@$NaYF_4$ (1.7 × 10^4 W/cm^2 compared to 0.95 × 10^4 W/cm^2). Notably, the four-order upconversion emission of Er was not detected in either nanoparticle while the characteristic emission of Gd at 311 nm was absent in the $NaGdF_4$:Yb, Er@$NaYF_4$.

References

1. M. Mousavi, B. Thomasson, M. Li, M. Kraft, C. Wurth, U. Resch-Genger and S. Andersson-Engels, *Physical Chemistry Chemical Physics*, 2017, **19**, 22016-22022.
2. M. Kaiser, C. Wurth, M. Kraft, I. Hyppanen, T. Soukka and U. Resch-Genger, *Nanoscale*, 2017, **9**, 10051-10058.
3. O. Dukhno, F. Przybilla, V. Muhr, M. Buchner, T. Hirsch and Y. Mely, *Nanoscale*, 2018, **10**, 15904-15910.
4. D. Ananias, M. Kostova, F. Paz, A. Ferreira, L. Carlos, J. Klinowski and J. Rocha, *Journal of the American Chemical Society*, 2004, **126**, 10410-10417.
5. D. Sendor, M. Hilder, T. Juestel, P. Junk and U. Kynast, *New Journal of Chemistry*, 2003, **27**, 1070-1077.
6. H. KE and E. BIRNBAUM, *Journal of Luminescence*, 1995, **63**, 9-17.
7. Y. Li, Y. Chang, Y. Chang, Y. Lin and C. Laing, *Journal of Physical Chemistry C*, 2007, **111**, 10682-10688.
8. B. Maliwal, Z. Gryczynski and J. Lakowicz, *Analytical Chemistry*, 2001, **73**, 4277-4285.
9. Q. Su, S. Han, X. Xie, H. Zhu, H. Chen, C. Chen, R. Liu, X. Chen, F. Wang and X. Liu, *Journal of the American Chemical Society*, 2012, **134**, 20849-20857.
10. F. Wang, R. Deng, J. Wang, Q. Wang, Y. Han, H. Zhu, X. Chen and X. Liu, *Nature Materials*, 2011, **10**, 968-973.
11. S. Han, X. Qin, Z. An, Y. Zhu, L. Liang, Y. Han, W. Huang and X. Liu, *Nature Communications*, 2016, **7**, 1-7.
12. F. Frenzel, C. Wurth, O. Dukhno, F. Przybilla, L. Wiesholler, V. Muhr, T. Hirsch, Y. Mely and U. Resch-Genger, *Nano Research*, 2021, **14**, 4107-4115.
13. M. Quintanilla, E. Hemmer, J. Marques-Hueso, S. Rohani, G. Lucchini, M. Wang, R. Zamani, V. Roddatis, A. Speghini, B. Richards and F. Vetrone, *Nanoscale*, 2022, **14**, 1492-1504.
14. M. Kraft, C. Wurth, V. Muhr, T. Hirsch and U. Resch-Genger, *Nano Research*, 2018, **11**, 6360-6374.